COPOLY(IMIDE SILOXANE) ABHESIVE MATERIALS WITH VARIED SILOXANE OLIGOMER LENGTH

Christopher J. Wohl[1,*], Brad M. Atkins[2], Marcus A. Belcher[1], John W. Connell[3]
[1]National Institute of Aerospace, Hampton, VA 23666-6147

[2]Langley Aerospace Research Summer Scholar (LARSS), NASA Langley Research Center, Hampton, VA 23681-2199

[3]NASA Langley Research Center, Hampton, VA 23681-2199

ABSTRACT

Incorporation of PDMS moieties into a polyimide matrix lowered the surface energy resulting in enhanced abhesive interactions. Polyimide siloxane materials were generated using amine-terminated PDMS oligomers of different lengths to study changes in surface migration behavior, phase segregation, mechanical, thermal, and optical properties. These materials were characterized using contact angle goniometry, tensile testing, and differential scanning calorimetry. The surface migration behavior of the PDMS component depended upon the siloxane molecular weight as indicated by distinct relationships between PDMS chain length and advancing water contact angles. Similar correlations were observed for percent elongation values obtained from tensile testing, while the addition of PDMS reduced the modulus. High fidelity topographical modification via laser ablation patterning further reduced the polyimide siloxane surface energy. Initial particulate adhesion testing experiments demonstrated that polyimide siloxane materials exhibited greater abhesive interactions relative to their respective homopolyimides.

* To whom correspondence should be addressed: christopher.j.wohl@nasa.gov, (757) 864-8074

1. INTRODUCTION

In this work, copoly(imide siloxane) materials were investigated for abhesive (non-stick) applications. The polyimide class of materials has been used prolifically due to their superior properties (moisture uptake, good electrical insulating properties, excellent thermal stability, and good mechanical properties).[1] Copoly(imide siloxane)s have been demonstrated to be of greater utility in specific applications due to the pairing of polyimide materials properties with those of the siloxane portion including: better processability, increased impact resistance, decreased dielectric constants,[2] and of greatest significance for this work, a reduction of the material's surface energy.[3] The surface energy of a material, γ, plays a pivotal role in determining the material's wettability, adhesive capability, propensity for particulate adhesion, and chemical resistance. Materials with high surface energies will be more easily wetted by incident solvents, be capable of greater adhesive bond strength with other substrates, and be more likely to accumulate surface contaminants (both chemical contamination and debris). Therefore, the generation of low surface energy materials is important for environments where

debris free non-adhesive surfaces are of paramount importance such as: microelectronics fabrication, marine biofouling, and other applications requiring maintenance of pristine surfaces. NASA's return to lunar exploration presents yet another application for low surface energy abhesive materials as the lunar environment poses major challenges to mission success.[4]

NASA, and the broader aerospace community, has planned to return to the Moon to achieve several milestones. NASA is currently extending the scientific understanding of the Moon and how it relates to the formation and history of our planet and will continue these efforts in the future. Experiments have been conducted to further understand the composition and topology of the Moon by several space agencies outside of NASA including: Chang'e-1 (Chinese National Space Administration), SELENE (Japan Aerospace Exploration Agency), Chandrayaan-1 (Indian Space Research Organization), and SMART-1 (European Space Agency). NASA has sent several satellites to the Moon recently and has verified the existence of water on the lunar surface through the impact of the Lunar Crater Observation and Sensing Satellite (LCROSS) vehicle which was simultaneously observed by the Lunar Reconnaissance Orbiter (LRO), the Hubble Telescope, and terrestrial observatories. These results corroborate those of previous missions from other space agencies. This world-wide effort to collect information about the Moon is in anticipation of planned robotic and manned missions to the lunar surface. What has been learned as a result of the Apollo missions (from 1969 to 1972, those corresponding to lunar landing missions; Apollo 11-17) and the recent activities described above is that the planned exploration and eventual habitation of the Moon will present an array of challenges to both short and long term missions. These challenges range from logistical to architectural to environmental.

The environmental issues that could negatively impact lunar surface missions include: temperature fluctuation, triboelectrification, energetic particle exposure, and the lunar dust itself. The lunar dust is classified as the portion of the surface regolith ranging in size from 50 μm and lower and is comprised of a diverse collection of mineralogical compositions. These particles are abrasive and highly porous.[5] Due to the lack of a substantial atmosphere, the lunar dust particles are likely to exist in a chemically activated state and be electrostatically charged.[6-8] Further, impact events on the lunar surface have resulted in generation and deposition of Fe^0 domains imparting magnetic properties into a significant portion of the lunar dust.[9] There is also evidence that the lunar dust has a dynamic component with the greatest degree of mobility occurring at the terminator, the separation between day and night sides of the lunar surface, due to the dramatic change in electrostatic potential present there.[10, 11] With these properties, the lunar dust presents a tremendous challenge for the successful completion of lunar missions, both manned and robotic (**Figure 1**). An approach involving materials to mitigate the hazard that lunar dust presents requires modification of a material's surface properties. To this end, low surface energy copoly(imide siloxane)s were generated with various siloxane segment lengths.

Figure 1. Apollo 17, Geologist-Astronaut Harrison Schmitt uses an adjustable sampling scoop. His suit is coated in lunar dust. (NASA JSC: AS17-137-20979)

2. EXPERIMENTATION

2.1 Materials

Prior to use, 2,2-bis(3,4-dicarboxyphenyl)hexafluoropropane dianhydride (6FDA, Clariant Corporation, T_m = 242 °C) was vacuum dried and 3,4'-oxydianiline (3,4'-ODA, Aldrich, T_m=71 °C) was vacuum distilled. 4,4'-oxydiphthalic anhydride (ODPA, Chriskev Company, Inc., T_m=226 °C), 4,4'-oxydianiline (4,4'-ODA, Wakayama Seika Kogya Co. Ltd, T_m=188 °C), 2,2-bis[4-(4-aminophenoxy)phenyl]hexafluoropropane (4-BDAF, Wakayama Seika Kogya Co. Ltd, T_m=162 °C), and aminopropyl-terminated siloxanes (Gelest) were used as received. The molecular weight of the siloxane materials was determined using ^{1}H NMR spectroscopy by calculating the ratio of methylene protons of the amino-propyl groups to the methyl groups on the siloxane repeat units. This type of end-group analysis typically has errors ≤ 5 %.[12] In some cases, the experimentally determined molecular weight differed significantly from the manufacturer's values (**Table 1**). Differential scanning calorimetry (DSC) was conducted using a Setaram Instrumentation DSC 131 with a heating rate of 20 °C/min. Polymer film mechanical properties were determined on a Sintech 2W with a cross-head speed of 5.08 mm/min. The data was collected and analyzed using Testworks 8.0. ^{1}H NMR spectra were recorded on a Bruker instrument operating at 300.152 MHz. Material surfaces were imaged using a Zeiss LSM 5 Exciter confocal microscope and an Olympus BH-2 optical microscope equipped with a Hitachi KP-D50 digital color camera. Water contact angle data was collected using a First Ten Angstroms FTA 1000B contact angle goniometer. Tilting axis contact angles were measured for each sample using an 8 μL water droplet. Interfacial tension measurements of a suspended water drop were made prior to experimentation to verify water purity and precision of the focused image. Contact angles were determined by drop shape analysis from a series of images collected at a rate of 2 frames/s. The stage of the contact angle instrument was tilted at a rate of 2 °/s to an inclination of 60°. A minimum of two measurements were recorded for each sample.

Table 1. Molecular weights for the siloxane materials.

Siloxane	Designation	Molecular Weight (g mol^{-1}) Reported	^{1}H NMR Analysis	Number of repeat units
Disiloxane	S1	249	249	1
DMS-A11	S2	875	1150	12
DMS-A15	S3	3000	2980	37
DMS-A21	S4	5000	6150	80
DMS-A32	S5	30000	35800	480

2.2 Polyimide Synthesis

Polyimides were prepared by the condensation reaction of stoichiometrically equivalent amounts of aromatic dianhydride and aromatic diamine (**Scheme 1**). The reaction vessel was flushed with nitrogen for 10 minutes prior to the addition of any reactants. Reactions were carried out under nitrogen at 20 wt. % solids in *N*-methylpyrrolidinone (NMP). The diamine was dissolved in NMP, to which the dianhydride was added, followed by additional NMP. The reaction mixture was mechanically stirred overnight.

Scheme 1. Polyimide synthesis and monomer structures. Common abbreviations for these monomers are adjacent to the structures.

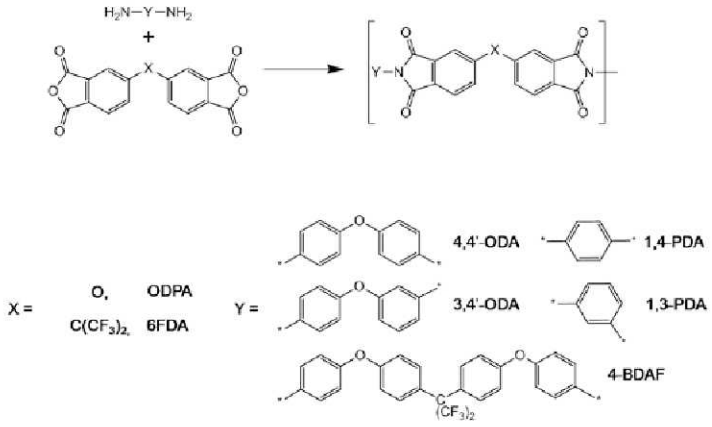

Copoly(imide siloxane)s were prepared similarly, except a solvent mixture of 4:1 NMP and tetrahydrofuran (THF) was used. The PDMS component (10 wt. % of the total solids) was dissolved in THF and added to the reaction vessel at the same time as the diamine (a representative structure is shown in **Scheme 2**). For brevity, the names of the copoly(imide siloxane)s generated here have been assigned designations corresponding to their monomeric composition. The designations for the siloxane component can be found in **Table 1** and the definition of the different polyimide monomeric compositions can be found in **Table 2**. For example, a polymer synthesized from 6FDA and 4,4'-ODA without the addition of a siloxane component would be assigned the designation P1S0, while a polymer comprised of the same two monomers with the addition of the PDMS with a molecular weight of 2980 g mol^{-1} would be labeled as P1S3. Inherent viscosities (η_{inh}) were determined at 25 °C on amide acid solutions using an Ubbelohde viscometer and solution concentrations of 0.5 g dL^{-1} (**Table 2**). Films were cast on glass plates or polished stainless steel using a doctor blade and placed in a forced air

drying chamber until "tack-free." Films were thermally imidized under nitrogen using a cure cycle with stages at 150, 175, 200, and 250 °C with at least a 40 min hold at each temperature.

Scheme 2. Copoly(imide siloxane) structure.

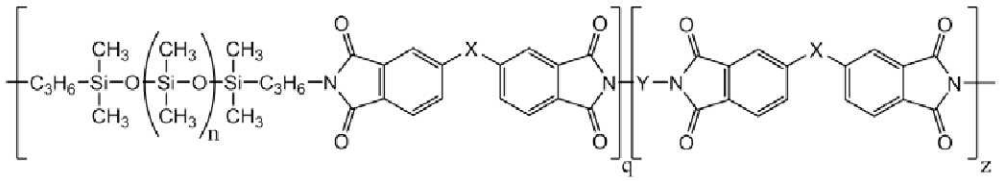

Table 2. Copoly(imide siloxane) designations and inherent viscosity values. For dianhydride and diamine structures, refer to Scheme 1.

Copolymer Designation	Dianhydride	Diamine	Siloxane Oligomer	η_{inh}, dL g^{-1}	Film Opacity
P1S0	6FDA	4,4'-ODA	None	1.42	Transparent
P1S1	6FDA	4,4'-ODA	Disiloxane	0.21	Transparent
P1S2	6FDA	4,4'-ODA	DMS-A11	0.91	Transparent
P1S3	6FDA	4,4'-ODA	DMS-A15	0.95	Opaque
P1S4	6FDA	4,4'-ODA	DMS-A21	1.28	Opaque
P1S5	6FDA	4,4'-ODA	DMS-A32	1.14	Opaque
P2S0	6FDA	3,4'-ODA	None	0.94	Transparent
P2S1	6FDA	3,4'-ODA	Disiloxane	0.33	Transparent
P2S2	6FDA	3,4'-ODA	DMS-A11	0.65	Opaque
P2S3	6FDA	3,4'-ODA	DMS-A15	0.76	Opaque
P2S4	6FDA	3,4'-ODA	DMS-A21	1.03	Opaque
P2S5	6FDA	3,4'-ODA	DMS-A32	0.86	Opaque
P3S0	6FDA	1,4-PDA	None	0.87	Transparent
P3S1	6FDA	1,4-PDA	Disiloxane	0.66	Transparent
P3S2	6FDA	1,4-PDA	DMS-A11	0.93	Transparent
P3S3	6FDA	1,4-PDA	DMS-A15	1.04	Opaque
P3S4	6FDA	1,4-PDA	DMS-A21	0.73	Opaque
P3S5	6FDA	1,4-PDA	DMS-A32	1.05	Opaque
P4S0	6FDA	1,3-PDA	None	0.74	Transparent
P4S1	6FDA	1,3-PDA	Disiloxane	0.53	Transparent
P4S2	6FDA	1,3-PDA	DMS-A11	0.76	Transparent
P4S3	6FDA	1,3-PDA	DMS-A15	0.66	Opaque
P4S4	6FDA	1,3-PDA	DMS-A21	0.35	Opaque
P4S5	6FDA	1,3-PDA	DMS-A32	0.67	Opaque
P5S0	6FDA	4-BDAF	None	1.18	Transparent
P5S1	6FDA	4-BDAF	Disiloxane	0.70	Transparent
P5S2	6FDA	4-BDAF	DMS-A11	0.95	Opaque
P5S3	6FDA	4-BDAF	DMS-A15	0.78	Opaque
P5S4	6FDA	4-BDAF	DMS-A21	1.28	Opaque
P5S5	6FDA	4-BDAF	DMS-A32	1.09	Opaque
P6S0	ODPA	4,4'-ODA	None	1.21	Transparent
P6S4	ODPA	4,4'-ODA	DMS-A21	0.50	Opaque

2.3 Laser Ablation Patterning

A 0°/90° crosshatch pattern was etched into polymer film surfaces (1 cm^2) using a PhotoMachining, Inc. laser ablation system equipped with a Coherent Avia® frequency-tripled Nd:YAG laser (λ = 355nm, 7 W). The laser beam energy, diameter, and scan speed were kept constant at 5.25 W, 25 μm and 25.4 cm/s, respectively, and line spacing was maintained at 25 μm.

2.4 Adhesion Testing

Particle adhesion testing was performed using an in-house device modeled after a similar instrument described in the literature.[13, 14] A polymer film sample was adhered to the end of a sonic wand tip (VCX-750, Sonics and Materials, Inc.) using an acrylic adhesive. Lunar dust simulant (NASA/USGS Lunar Highland simulant, maximum particle diameter < 30 μm) was deposited on the polymer surface by placing the polymer film in a plastic bag containing the simulant. Agitation of the bag caused simulant to become airborne and deposit on the film surface. The sonic wand was then suspended over a laser optical particle counter (Solair 3100, Lighthouse Worldwide Solutions) in either a vertical (**Figure 2A**) or a horizontal (**Figure 2B**) configuration, with the entire assembly housed in a vacuum chamber (Abbess Instruments). By variation of the sonic wand's vibrational amplitude, particles were dislodged from the polymer film and gravitationally fed into the optical particle counter where size distribution was determined. Activation of the sonic wand induced vibration at the tip that resulted in an acceleration force acting normal to the sample plane, F_{sw}, determined by the acceleration of the tip, a, the frequency of oscillation, ω, and the amplitude of displacement, A. Particles adhered to the surface were dislodged when the sonic wand acceleration force, F_{sw}, exceeded the adhesion force, F_{adh} (**Eq. 1**).

$$F_{sw} = ma = m(4\pi^2\omega^2 A) > F_{adh} \quad [1]$$

where m is the dislodged particle's mass. For measurements conducted in the vertical orientation (**Figure 2A**), gravitational forces acting normal to the plane were considered. In the horizontal configuration, this term would be further complicated by friction between the particles and the polymer film surface and therefore was not included in calculations. The particles were assumed to be spherical with a density of 2.9 g cm^{-3}. A protocol was established to test the adhesion force of particles to a sample surface by variation of sonic wand amplitude from 20 – 80 % corresponding to surface acceleration values from 380 – 1550 km s^{-2}. Adhesion force values were calculated according to the size of the particles detected in the optical particle counter. After the adhesion testing was completed, samples were removed from the device assembly and observed under the optical microscope to identify the particles still adhered to the surface. For the surfaces investigated here, particles remained on the surface upon completion of the experiments and the adhesion forces calculated for these particles were lower boundary adhesion force values.

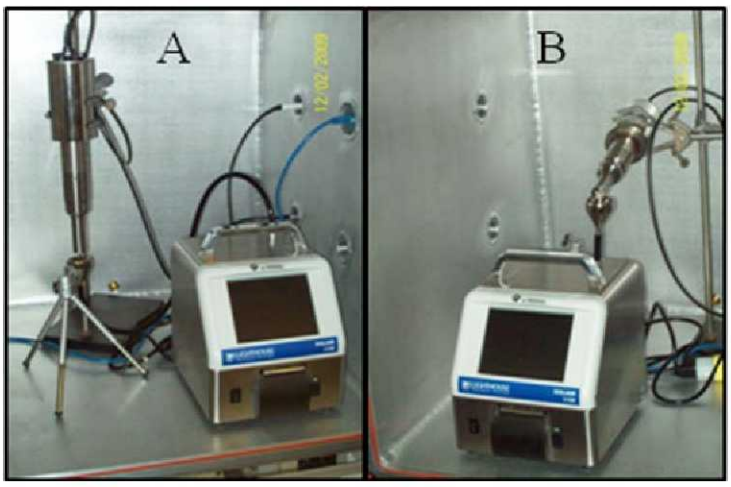

Figure 2. Images of the adhesion testing device in the vertical (**A**) and horizontal (**B**) configurations.

3. RESULTS AND DISCUSSION

3.1 Polymer Synthesis and Characterization

Copoly(imide siloxane)s were synthesized for the purposes of generating low surface energy materials for abhesive applications. The siloxane oligomer length was varied to investigate the domain formation/phase segregation and surface migration behavior of the siloxane moieties as it related to siloxane size. Although the polymerization reactions were undertaken the same way, the relative degree of polymerization and average molecular weight can be inferred from inherent viscosity values (**Table 2**). The addition of disiloxane always led to a reduction in the inherent viscosity of the polyamide acid solution. The incorporation of smaller siloxane moieties was found to preserve the transparency of the copolymer film, while incorporation of siloxane oligomers 2980 g mol^{-1} or higher resulted in an opaque film, suggesting that the copolymer was phase segregated (**Table 2**). Phase segregation in similar copolymers was observed using electron microscopy and small angle neutron scattering to visualize the segregated domains.[15] Further evidence for this was observed in the thermal and mechanical analysis of these materials.

3.1.1 Thermal Properties

The thermal properties of a material often provide insight into structuring and long range order phenomena within the bulk material. DSC was used to understand how the incorporation of siloxane oligomers affected these processes within a polyimide matrix. The change in heat capacity upon progression through the glass transition temperature, T_g, was not significant for some of the homopolyimides generated here making detection by DSC difficult. This problem was exacerbated upon the addition of siloxane moieties, resulting in the absence of a detectable glass transition temperature for some of the copoly(imide siloxane) materials. In several instances, however, reliable data was collected for a full series of materials. For example, T_g was found to decrease for all polyimide compositions studied here up to 14% (a change of 39 °C) as a result of incorporation of the siloxane S4 (MW = 6150 g mol^{-1}).

Similarly, T_g values varied significantly depending on which siloxane oligomer was present in the copoly(imide siloxane). Smaller siloxane moieties resulted in dramatic reductions in T_g values, while larger siloxane components resulted in less dramatic changes (**Figure 3**). This is further evidence that the larger siloxane oligomers exhibited greater phase separation within the polyimide matrix, which is in agreement with the differences in film transparency. The change in heat capacity for a series of copoly(styrene siloxane) materials indicated that the degree of phase mixing (**DPM)** was dependant on siloxane segment lengths (with larger segment lengths exhibited lower DPM values) similar to the results presented here.[16] If the two polymers were miscible, the addition of siloxanes should reduce the T_g according to the Fox equation (which relates a copolymer's T_g to the relative weight percentages and T_g for each hompolymer). Although the weight percent of the siloxane containing polyimide portion should be slightly reduced due to the reduced number of amine functionalities for the larger siloxanes, the difference in the calculated T_g values does not correlate with the data collected for these materials. Although it appears that incorporation of larger siloxane moieties resulted in increased T_g values approaching the homopolyimide's T_g, the data suggested that further increasing the size of the siloxane moiety would not result in a copolymer with the same T_g as the homopolyimide. This behavior is possibly due to a reduction in T_g values as a rule of mixtures for these two materials instead of actual disruption of intermolecular forces as appears to be the case for smaller siloxanes. Phase transitions arising from the siloxane moieties themselves would not have been observable in the experiments conducted here because their T_g values are well below room temperature (typically < -120 °C).

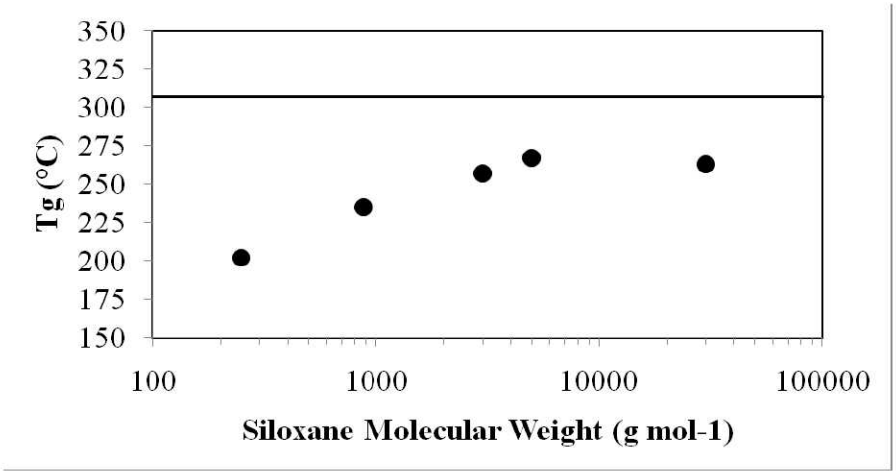

Figure 3. T_g values for the **P5S** copoly(imide siloxane)s. The line on the graph corresponds to the T_g value for the homopolyimide (307 °C). Note: the x-axis is displayed on a logarithmic scale for clarity.

3.1.2 Mechanical Properties

The addition of siloxane moieties resulted in a decrease in the modulus for all of the investigated polyimide matrices (**Figure 4A**). Furthermore, within each polyimide type, larger siloxane functionalities resulted in greater reductions in modulus, possibly due to increased disruption of the polyimide domains (the major contributor to the modulus). The trend observed in this data

suggests that a minimal modulus value (approximately 75% of the homopolyimide value) is obtained upon increase of the siloxane molecular weight to 6150 g mol^{-1}.

Another important mechanical parameter for the materials discussed here is the ultimate percent elongation, which is an indicator of the elastic/inelastic deformation capability of the polymeric material (**Figure 4B**). The addition of siloxane moieties increased the elastic/inelastic deformation length for all of the polyimide matrices studied here. The data is displayed as change in the percent elongation values relative to the corresponding homopolyimide material due to the large disparity between polyimide matrices. For example, materials generated from the P2 polyimide matrix exhibited percent elongation values of 8.9 and 18.5 % for siloxanes S0 and S3, respectively, while the P3 materials elongated 2.7 and 9.7 % for the same siloxane additions. Again, the effects of phase segregation are observed. For copolymers containing low molecular weight siloxanes, the percent elongation value is considerably larger than the homopolymer (as high as 290%). Increased siloxane molecular weight actually results in a decrease in this effect with copolymers containing the S5 siloxane demonstrating the lowest increase in % elongation. One caveat to this interpretation is that changes in morphology could result in some of the observed thermal and mechanical behavior of these copolymers. Experiments are currently underway to visualize and quantify the phase segregation behaviors for these copoly(imide siloxane) materials.

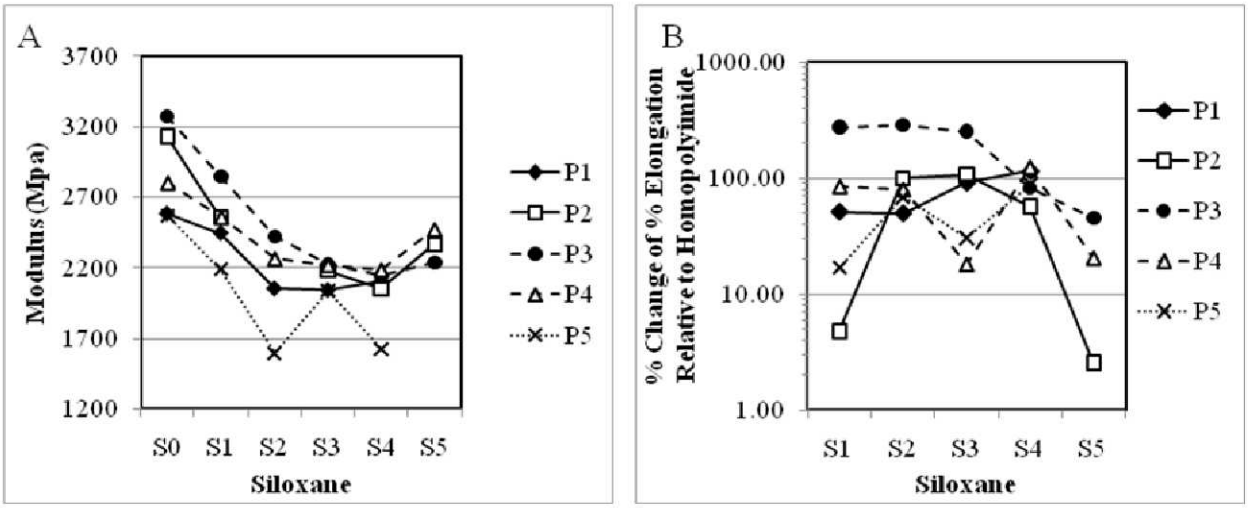

Figure 4. (A) The modulus for all copolymers indicated a reduction with increased siloxane molecular weight. (B) The change in percent elongation for materials relative to homopolyimides indicated that increased domain formation from incorporation of larger siloxane moieties reduced the gain in elastic/inelastic deformation from siloxane incorporation. Note: the y-axis in (B) is logarithmic for clarity.

3.1.3 Contact Angle Analysis

The surface energy of a material is one of several indicators of the likelihood for adhesive interaction with contaminants through non-mechanical interactions (chemical vs. physical attachment), where surfaces with lower surface energies would be anticipated to exhibit reduced adhesive interactions. The surface energy of a material can be determined by measuring the

contact angle that solvents of known surface tension make with an interrogated surface. Higher contact angle values correlate with lower surface energies. Water contact angles were collected from images of 8 μL drops deposited on the copolymer film surfaces, which were subsequently subjected to tilting angles up to 60° (**Figure 5**). Advancing water contact angle values, θ_{adv}, indicated that increased siloxane molecular weight resulted in greater θ_{adv} values. Copoly(imide siloxane)s generated with the S5 siloxane (Mw = 35,800 g mol^{-1}) exhibited the greatest θ_{adv} values and in some cases surpassed that of Teflon® (θ_{adv} ~ 110°). This increase in θ_{adv} values suggests a preferential orientation of the siloxane moieties to the polymer surface. The data also suggested that θ_{adv} could increase further via incorporation of larger siloxane moieties; however, this is unlikely due to the balance between gravitational forces, cohesive forces within the water drop, and interfacial interactions. A further reduction in the surface energy required a reduction in the interaction area which was achieved via topographical modification as described below.

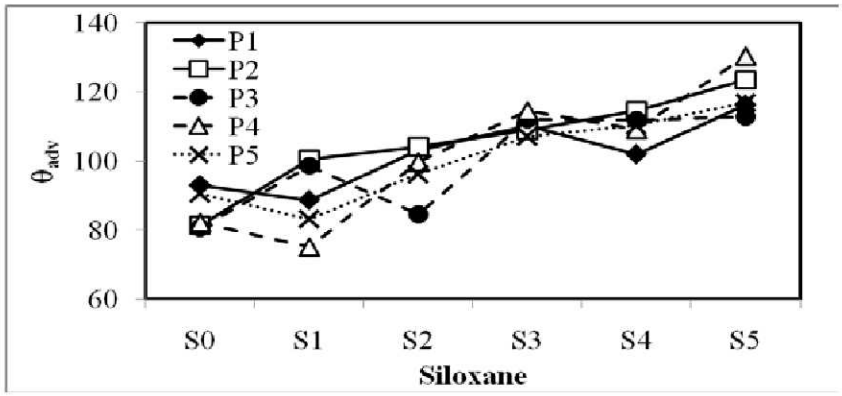

Figure 5. Contact angle data for copoly(imide siloxane) materials. Increasing the molecular weight of the siloxane moiety resulted in increased θ_{adv} values. The observed change was similar for all polyimide formulations investigated here.

3.2 Laser Ablation Patterning

As contact angles indicated (**Figure 5**), generation of copoly(imide siloxane) materials greatly reduced the material's surface energy and implicitly, the propensity of particulate contamination. To increase θ_{adv} values even more (and further reduce the surface energy), the surfaces were topographically modified using laser ablation patterning. Laser patterning affords a precise, high-fidelity process with several adjustable parameters enabling transcription of a variety of patterns and variation thereof. A simple 0°/90° cross-hatch pattern was utilized here. In previous work, a series of experiments were performed to determine the appropriate laser parameters to impart topographies on the copolymer film surfaces.[17] The settings necessary to generate topographical features several microns in height were determined to be 5.25 W laser pulses with a frequency of 80 kHz and a scan speed of 25.4 cm s^{-1}. The cross-hatch pattern was transcribed onto the surface four times to increase the ablation depth. Highly accurate sample alignment enabled several transcription steps to be performed on a sample surface with nearly exact overlap of previous steps. Optical and confocal micrographs verify the fidelity of this process over large length scales (**Figure 6**). Although not shown here, this approach was adopted to transcribe patterns into copoly(imide siloxane) films on length scales of several centimeters.

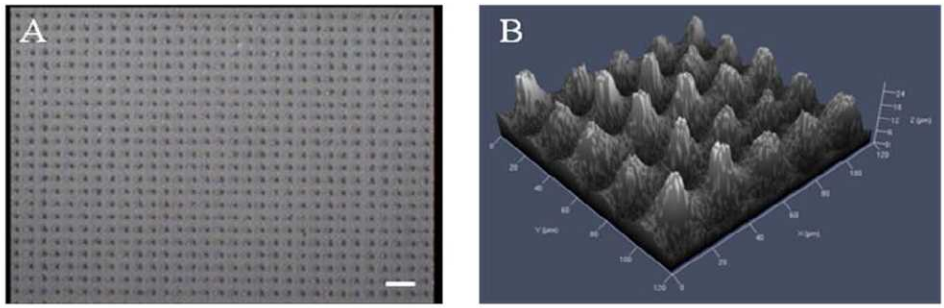

Figure 6. Optical (A) and confocal (B) micrographs of a laser ablation patterned P2S3 surface. The scale bar in A is 50 μm.

The introduction of topographies resulted in increased water θ_{adv} values for all materials investigated here. **Figure 7** provides an example of the increase in θ_{adv} values for a hompolyimide (P1S0, top) and a copoly(imide siloxane) (P1S4, bottom). The increase in θ_{adv} was greater for the copolymeric materials than for the homopolyimide surfaces except for copolymers that incorporated the S1 siloxane. θ_{adv} values determined for the laser ablation patterned surfaces were classified as superhydrophobic ($\theta_{adv} \geq 150°$) and in some cases approached 180°. The θ_{adv} values for several copoly(imide siloxane)s are shown in **Figure 8**. Roll-off angles are further indications of the propensity of particles to adhere to surfaces, with a low roll-off angle indicating the incident solvent does not wet the surface. If the material exhibits a shallow roll off angle, presumably a shallow tilting angle would be required to remove contaminating particles. Although large θ_{adv} values are indicative of low surface energies, there are examples in the literature where water droplets strongly adhered to a superhydrophobic surface.[18] Although not shown, the roll-off angles for several laser ablation patterned copoly(imide siloxane)s were < 10°, with roll-off angles as low as 2° observed suggesting that laser ablation patterned copoly(imide siloxane) surfaces should exhibit greater mitigation capabilities of particulate adhesion compared to non-patterned surfaces.

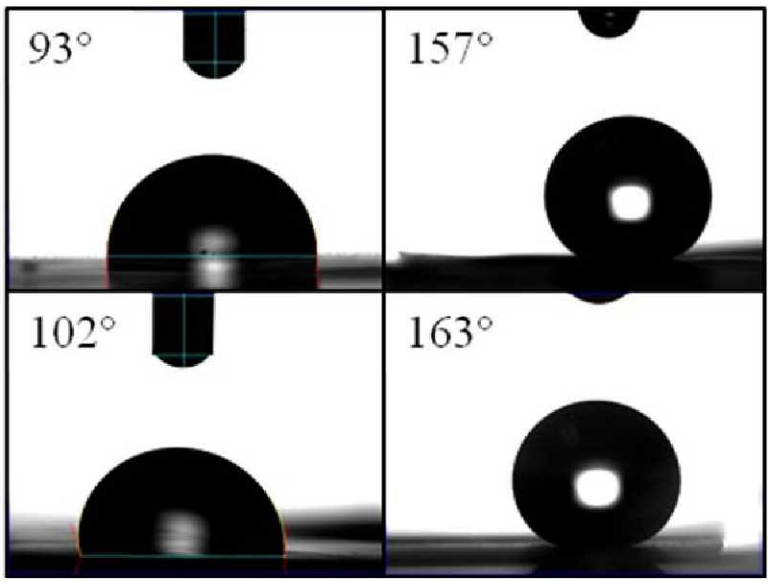

Figure 7. Images of water drops used to determine contact angles observed on P1S0 (top, homopolyimide) and P1S4 (bottom, copoly(imide siloxane)) before (left) and after (right) laser ablation patterning.

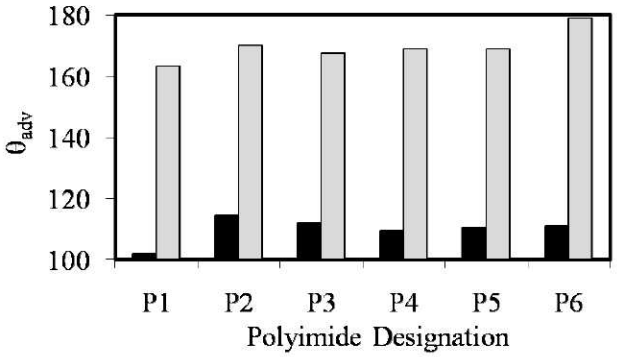

Figure 8. Contact angle comparison of pristine copoly(imide siloxane) surfaces (black) with laser ablation patterned surfaces (gray). All of the data corresponds to copolymers generated with S4 except for P3 and P4 which contain the S3 siloxane moiety.

3.3 Particle Adhesion Testing

A more direct method to evaluate the efficacy of the generated copoly(imide siloxane) materials for abhesive applications was to test particulate adhesion itself. To do this, a device was generated based on a previous instrument to measure the retention of particulate matter on an intentionally contaminated surface after the application of external stimulus (**Figure 2**).[13] The external stimulus was provided by sonication of a polymer film sample, coated with lunar simulant, affixed to the end of a sonic wand. Dislodged particles were collected and sized in a laser optical particle counter. The size of these particles was then used to calculate an adhesion force based on the amplitude setting of the sonic wand (**see Eq. 1**). For comparative purposes, a

commercially available polyimide (Kapton® HN) was tested along with a copoly(imide siloxane) and a laser ablation patterned copolymer sample. After completion of the sonic wand amplitude protocol, each sample demonstrated retention of particulate matter (i.e., $F_{adh} \geq F_{sw}$, **Figure 9**). The size of particles on the surface was determined using optical microscopy and a lower bound for the adhesion force was calculated. The particle count and adhesion force for each surface is indicated in **Table 3**. The copoly(imide siloxane) material had a demonstrated decrease in both particle count and adhesion force relative to Kapton® HN. Laser ablation patterning further reduced the number of adhered particles and the adhesion force.

Figure 9. Sonic wand adhesion testing indicated that the polyimide surface (**A**) retained a greater number of particles than the copoly(imide siloxane) surface both before (**B**) and after laser ablation patterning (**C**). The lunar simulant particle retained on the laser ablation patterned surface can be seen near the center of the image. The scale bar is 25 μm.

Table 3. Preliminary adhesion testing results.

Material	Particle Count	Adhesion Force, nN
Kapton® HN	~378	156
P1S4	~252	112
Laser Patterned P1S4	1 - 2	10 - 68

4. CONCLUSIONS

In this work, low surface energy copoly(imide siloxane)s were generated with various siloxane segment lengths. Characterization of these materials revealed that domain formation of the low surface energy component within the matrix was more prevalent for longer siloxane segments as indicated by increased opacity, decreased mechanical properties and variation of the glass transition temperature, T_g. Incorporation of siloxanes lowered the polymer's surface energy as indicated by water contact angle values. Topographical modification of these materials by laser ablation patterning further reduced the surface energy and in some cases generated superhydrophobic surfaces.

Combined, the contact angle data and particle adhesion testing indicate that copoly(imide siloxane) materials may provide greater mitigation to particulate adhesion than polyimide materials alone. These enhanced surface properties for abhesive applications were generated to the detriment of the polymers' moduli. It is possible that lower siloxane loading levels would result in retention of the mechanical properties of the polyimide while still affording abhesive surface properties and this approach is currently being investigated. Laser ablation patterning offers further reduction in particle retention as the available surface area for particle adhesion is reduced. Pattern variation and size dependencies are currently being evaluated.

For the purposes of lunar dust adhesion mitigation, it is likely that this approach, termed passive due to the lack of input from an external energy source, would not be sufficient to mitigate surface contamination or clean contaminated surfaces for some lunar applications. It is feasible that combining these materials with active mitigation strategies - methods that utilize input from external energy sources - would broaden the applicability of such materials for abhesive purposes. Collaborative efforts along these lines have been initiated with researchers at NASA Kennedy Space Center where experiments are being conducted involving a series of embedded electrodes within polymeric matrices.[19]

5. ACKNOWLEDGEMENTS

The authors would like to thank Professor Michael E. Mullins, Michigan Tech, for discussions concerning the manufacture of the particle adhesion testing device and Dr. Jeffrey A. Hinkley for scientific discussion. This work was funded through the NASA Langley Research Center's Creative and Innovative Research Fund.

6. REFERENCES

1. Polyimides. New York: Chapman and Hall, 1990.

2. Mahoney, C., et al. "Surface characterization and adhesive properties of poly(imidesiloxane) copolymers containing multiple siloxane segment lengths." Macromolecules *35* (2002):5256 - 5266.

3. Park, H., et al. "Effect of a UV/ozone treatment on siloxane-containing copolyimides: surface modification and gas transport characteristics." Chem. Mater. *15* (2003):2346 - 2353.

4. Taylor, Lawrence, et al. "The Lunar Dust Problem: From Liability to Asset." *1st Space Exploration Conference: Continuing the Voyage of Discovery* Orlando, Florida, January 30 - February 1 (2005).

5. Colwell, J. E., et al. "Lunar surface: dust dynamics and regolith mechanics." Review of Geophysics *45* (2007):2005RG000184.

6. Abbas, M., et al. "Lunar dust charging by photoelectric emissions." Planetary Space Sci. *55* (2007):953 - 965.

7. Halekas, J., et al. "Large negative lunar surface potentials in sinlight and shadow." Geophysical Research Letters *32* (2007):L09102.

8. Sternovsky, Zoltan; and Robertson, Scott. "Contact charging of lunar and martian dust simulants." Journal of Geophysical Research *107* (2002):15-11 - 15-18.

9. Taylor, Lawrence and Meek, Thomas. "Microwave Sintering of Lunar Soil: Properties, Theory, and Practice." J. Aerospace Eng. *18* (2005):188 - 196.

10. Borisov, N. and Mall, U. "Charging and motion of lunar dust grains near the terminator of the Moon." Planetary Space Sci. *54* (2006):572 - 580.

11. Stubbs, Timothy;, et al. "A dynamic fountain model for lunar dust." Adv. Space Res. *37* (2006):59 - 66.

12. Hatada, K. and Kitayama, T. NMR Spectroscopy of Polymers. Berlin, Germany: Springer Verlag, 2004.

13. Mullins, M., et al. "Effect of geometry on particle adhesion." Aerosol Sci. Technol. *17* (1992):105 - 118.

14. Zimon, A. Adhesion of Dust and Powder. New York: Plenum Press, 1969.

15. Samseth, J., et al. "Effect of molecular architecture on microstructural characteristics in some polysiloxaneimide multiblock copolymers." J. Appl. Polym. Sci. *44* (1992):1245-1256.

16. Feng, D., et al. "Structure-property behavior of free radical synthesized polydimethylsiloxane-polystyrene multiblock polymers: 1. Effect of the siloxane block length." Polymer *30* (1989):1800 - 1813.

17. Wohl, Christopher J., et al. "Superhydrophobic polyimide siloxane surfaces generated via laser ablation patterning." manuscript in preparation.

18. Winkleman, A., et al. "Immobilizing a drop of water: fabricating highly hydrophobic surfaces that pin water." Nanoletters *8* (2008):1241 - 1245.

19. Immer, C., et al. "Electrostatic Screen for Transport of Martian and Lunar Regolith." *Lunar and Planetary Science XXXVII* Houston, March 13-17 (2006).